

# Molecular Layer Deposition for Surface Modification of Lithium-Ion Battery Electrodes

Chunmei Ban\* and Steven M. George\*

Inspired by recent successes in applying molecular layer deposition (MLD) to stabilize lithium-ion (Li-ion) electrodes, this review presents the MLD process and its outstanding attributes for electrochemical applications. The review discusses various MLD materials and their implementation in Li-ion electrodes. The rationale behind these emerging uses of MLD is examined to motivate future efforts on the fundamental understanding of interphase chemistry and the development of new materials for enhanced electrochemical performance.

## 1. Introduction

Extensive research has been performed on lithium-ion (Li-ion) batteries ever since the first paper demonstrated a functioning rechargeable Li-ion battery based on intercalation.<sup>[1]</sup> The successful commercialization of the Li-ion battery by Sony led to the explosion of the portable electronics market. With growing attention to reducing fossil fuel dependence and greenhouse gas emissions, efforts have been expanded to address the increasing environmental needs for energy storage systems that can be coupled with renewable energy, such as solar and wind technologies, to implement electric vehicles. The desire to electrify transportation and realize large-scale grid storage has intensified the search for new electrode materials having increased energy density. In addition, strategies are needed to stabilize electrode materials from uncontrolled deleterious side reactions, thus leading to improved safety and long lifetime. These issues of safety and lifetime are essential for the commercial success of Li-ion batteries in all applications.

The surface of electrode materials plays a critical role in the electrochemical behavior of electrode materials. The stability and reactivity of the surface and interphases dominate

the performance of electrochemical systems.<sup>[2–4]</sup> Surface modifications that chemically or physically change the surface of electrode components have been shown to improve significantly the interface chemistry, conductivity, and mechanical integrity in Li-ion electrodes.<sup>[5–10]</sup> Traditionally, coatings have been formed from the solution phase using spin-coating and other wet processes. However, there are problems in obtaining uniformity in very thin films from solution deposition. In

particular, achieving conformal coatings is especially difficult on substrates with high-aspect-ratio features.

To overcome the challenges associated with wet processes, dry processes, such as chemical vapor deposition can be used to form thin films. Among the dry processes, atomic layer deposition (ALD), which is based on sequential and self-limiting surface reactions, has proven to be the best method to deposit continuous, conformal, and pinhole-free films with superb control over film thickness, composition, and conformality at the atomic level.<sup>[11,12]</sup> ALD has been used to fabricate various inorganic materials, such as binary oxides, sulfides, and nitrides.<sup>[12,13]</sup> Previous work has demonstrated that ALD is an important tool to modify the surface of electrodes. ALD coatings can mitigate the parasitic side reactions between the liquid electrolyte and the surface of electrodes, and lead to the improved performance of Li-ion electrodes.<sup>[8,10,14]</sup>

The quest for high-capacity Li-ion electrodes led to the use of silicon (Si) and silicon-based alloy anode materials because of the superior theoretical Li storage capacity of silicon.<sup>[15–17]</sup> The Si anode represents a new type of Li-ion electrode that is based on reversible alloy/de-alloy reactions and exhibits high volumetric changes accompanying Li-ion charging and discharging.<sup>[18–20]</sup> Silicon-based electrodes require that the coating materials are chemically stable and also sufficiently robust to allow volumetric expansion. Rigid inorganic coatings such as Al<sub>2</sub>O<sub>3</sub> do not satisfy the new needs for high-capacity, high-volume-expansion silicon electrodes. Coating materials with improved mechanical properties are required to realize these promising electrode materials for next-generation Li-ion batteries.

In parallel, the continuous development of ALD techniques has fundamentally broadened the range of possible materials. Initially, only inorganic materials were deposited by ALD. In the 1990s, organic polymers were deposited by a variant of ALD, now commonly known as molecular layer deposition (MLD).<sup>[21]</sup> Subsequently, in the 2000s, a breakthrough was made to combine ALD precursors and all-organic precursors to produce organic-inorganic hybrid materials.<sup>[22,23]</sup> The MLD of

Dr. C. Ban  
Center of Chemistry and Nanoscience  
National Renewable Energy Laboratory  
Golden, CO 80401, USA  
E-mail: chunmei.ban@nrel.gov

Prof. S. M. George  
Department of Chemistry and Biochemistry  
University of Colorado at Boulder  
Boulder, CO 80309, USA  
E-mail: steven.george@colorado.edu

Prof. S. M. George  
Department of Mechanical Engineering  
University of Colorado at Boulder  
Boulder, CO 80309, USA



DOI: 10.1002/admi.201600762

hybrid organic-inorganic hybrid materials enables the synthesis of totally new materials families with versatile characteristics that are not possible by any other existing techniques.<sup>[24,25]</sup>

Developing durable electrode materials with high energy density requires functional and stable interphases that mitigate deleterious side reactions, reduce the loss of inventory lithium, and also ensure mechanical integrity through electrochemical reactions. Surface modification via ALD and MLD has been recognized as one of the most effective means to alter the surface chemistry and enable the formation of effective interphases on porous electrodes that have high surface area and high aspect ratio. Applying the emerging MLD technique for surface modification may offer significant improvements for electrodes with super high capacity for future Li-based batteries. Many reviews have already addressed the ALD technique and its applications for Li-ion batteries.<sup>[11,26]</sup> This review focuses on the new strategy of using the MLD method to stabilize the surface of high-capacity and high-volume-expansion electrode materials.

## 2. Molecular Layer Deposition of Ultrathin Films

The original work on MLD dates back to early work by Yoshimura in 1991 on pure organic polyimide polymer.<sup>[21,27]</sup> Analogous to ALD, MLD inherits the advantages of ALD with respect to uniformity, conformality, and controllability.<sup>[11]</sup> In addition, MLD significantly expands the selection of precursors and final products. Various organic polymeric materials—including polyimide, polyamide, polyurea, and cross-linked carbosiloxane—have been synthesized using all-organic precursors based on condensation polymerization reactions.<sup>[28–32]</sup> By combining all-organic precursors and the inorganic precursors used in the ALD process, MLD also enables the fabrication of a huge variety of hybrid organic-inorganic materials.<sup>[23,24]</sup> Several recent reviews have summarized the MLD of organic and hybrid organic-inorganic films.<sup>[33,34]</sup>

### 2.1. MLD of Organic Polymers

Polymer coatings are conventionally fabricated from the solution phase using spin-coating and other wet processes. Unfortunately, these solution methods have difficulty obtaining uniform polymer films at very small thicknesses. Achieving conformal coatings on substrates with high-aspect-ratio features is especially difficult. In contrast, dry processes are able to deposit polymeric thin films while avoiding non-wetting and surface-tension effects.<sup>[35]</sup> The dry process of MLD is based on sequential and self-limiting surface reactions,<sup>[23]</sup> that provide exquisite control over film thickness, composition, and conformality at the molecular level.

To provide an example of polymer MLD, **Figure 1** illustrates one MLD scheme to synthesize poly(p-phenylene terephthalamide) (PPTA) film on a substrate.<sup>[29]</sup> Before depositing the PPTA film, the initial surface was activated with amine groups from surface functionalization reactions with aminopropyltrimethoxysilane or ethanolamine. Subsequently, two precursors—terephthaloyl chloride (TC) and p-phenylene-diamine (PD)—were dosed sequentially with a purging step following



**Chunmei Ban** received her B.S. and Master degrees in Chemical Engineering and Electrochemistry from Tianjin University in 2000 and 2003. She earned Ph.D. from the State University of New York at Binghamton in 2008, followed by work as a Postdoctoral Fellow at the National Renewable Energy Laboratory (NREL).

She became a scientist in the Center of Chemistry and Nanoscience at NREL in 2012. Her current research focuses on electrochemistry and materials research of electrode materials for next-generation electrochemical batteries, as well as interfacial chemistry for stabilizing the interface between electrodes and electrolytes.



**Steven M. George** is Professor in the Dept. of Chemistry and Dept. of Mechanical Engineering at the University of Colorado at Boulder. He received his B.S. in Chemistry from Yale University and his Ph.D. in Chemistry from the University of California at Berkeley. His current research interests focus on atomic layer deposition (ALD), atomic layer etching (ALE) and molecular layer deposition (MLD). He has been particularly interested in developing new surface chemistry and applications for ALD and MLD. The electrochemical applications for ALD and MLD take advantage of the ability of ALD and MLD to deposit ultrathin and conformal films on high surface area substrates.

each dose to remove excess precursor from the reactor. During each reaction, the bifunctional monomer (TC or PD) reacts with the surface reactive groups resulting from the previous exposure. Each MLD cycle adds a molecular fragment to the growing film and leaves the surface terminated with new reactive sites for further film growth.

The versatility of the MLD chemistry enables unprecedented control of composition in the deposited organic film. MLD also allows synthesis of organic films at low temperature. Polyurea films have been grown at room temperature using MLD with isocyanate-amine urea coupling chemistry.<sup>[34]</sup> The transmission electron microscopy (TEM) images in **Figure 2a** show the uniform polyurea MLD films without the presence of voids and aggregates.<sup>[34]</sup> **Figure 2b** compares the transmission Fourier transform infrared (FTIR) spectra for polyurea MLD films with different numbers of MLD cycles and a density functional theory (DFT)-calculated spectrum of the repeating unit of the polyurea oligomer.<sup>[34]</sup> The notable difference is the red-shifting

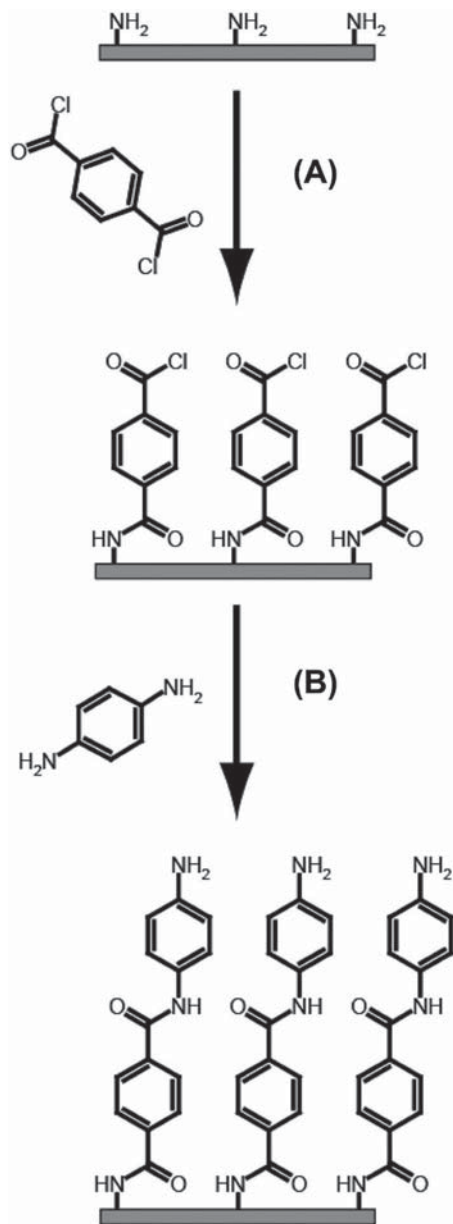


**Figure 1.** Schematic illustration of surface chemistry for PPTA MLD. In the “A” reaction, TC reacts with amine surface groups to form an amide linkage. In the “B” reaction, PD reacts with acid chloride surface groups to form an amide linkage. Reproduced with permission.<sup>[29]</sup> Copyright 2008, American Chemical Society.

of the stretching modes for the carbonyl oxygen group because of hydrogen bonding between the amide N–H group and the carbonyl oxygen of the adjacent chain. The self-limiting monolayer deposition results in a well-ordered hydrogen-bonded polyurea film.

## 2.2. MLD of Hybrid Organic-Inorganic Polymers

The combination of all-organic precursors and metal ALD precursors creates new possibilities for growing hybrid

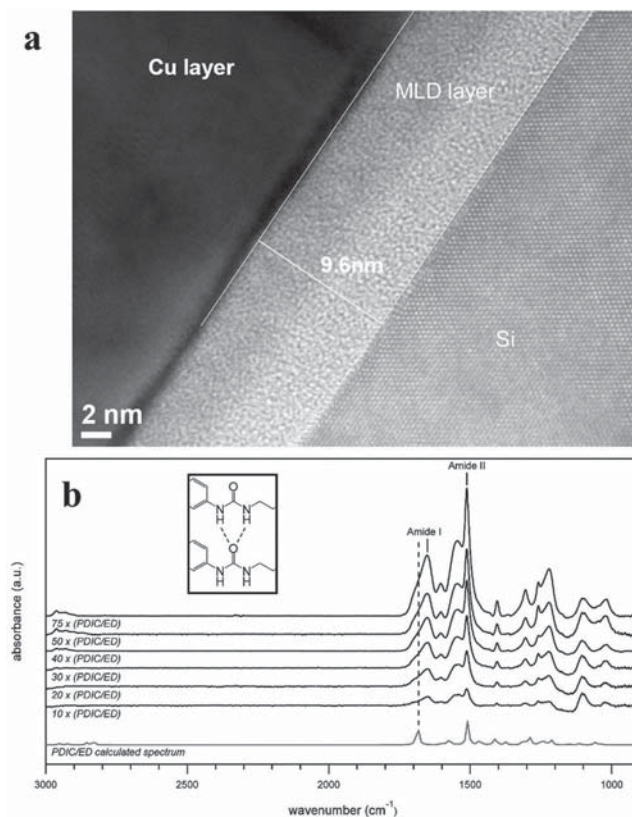


**Figure 2.** (a) TEM image of the uniform polyurea MLD film. (b) FTIR spectra of the polyurea MLD film with different number of MLD cycles and a spectrum calculated using DFT. Reproduced with permission.<sup>[34]</sup> Copyright 2010, American Chemical Society.

organic-inorganic materials with a wide spectrum of properties for various applications.<sup>[33]</sup> One important branch in hybrid organic-inorganic materials is the metal alkoxides, or metalcones, which are grown from metal precursors and various organic alcohols.<sup>[24,36]</sup> Aluminum alkoxides, or alucones, are the most extensively studied organic-inorganic films deposited by MLD.<sup>[22]</sup> Other metalcones that have been deposited include zirconone,<sup>[37]</sup> titanone,<sup>[38]</sup> zirconone<sup>[39]</sup> and hafniconone.<sup>[40]</sup>

The first alucone, designated as ALEG, was deposited based on trimethylaluminum (TMA) and ethylene glycol (EG).<sup>[22]</sup> Instead of using water in the Al<sub>2</sub>O<sub>3</sub> ALD process, the EG molecule, HO–CH<sub>2</sub>–CH<sub>2</sub>–OH, which contains two hydroxyl groups, is used in alucone ALEG MLD to integrate –O–CH<sub>2</sub>–CH<sub>2</sub>–O– fragments between aluminum centers. Polyols, such as glycerol (GL), have also been used to ensure the availability of hydroxyl groups for the subsequent TMA exposure.<sup>[6,36]</sup>

**Figure 3** illustrates the scheme of alucone AlGL MLD via the reactions with TMA and GL. The surface chemistry is based on the reaction between surface hydroxyl groups and TMA and the reaction between the AlCH<sub>3</sub><sup>\*</sup> surface species and GL according to:



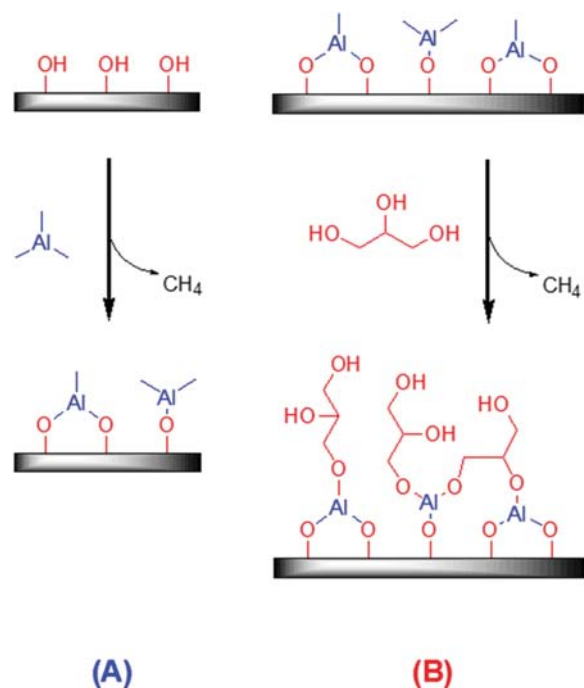


**Figure 3.** Schematic illustration of alucone AIGL MLD based on the reaction between surface hydroxyl groups with TMA and the reaction between  $\text{AlCH}_3^*$  surface species with GL. Reproduced with permission.<sup>[6]</sup>

where the asterisks indicate the surface species and R represents the organic fragment incorporated from GL. Because of the presence of more than two hydroxyl groups per GL molecule, sequential reactions between  $\text{Al}(\text{CH}_3)_3$  and GL produce high degrees of crosslinking between polymer chains that strengthen the alucone films and lead to higher fracture toughness.

The growth rate for the AIGL MLD process is known to be 2.5 Å per AB cycle at a substrate temperature of 140 °C.<sup>[6,41]</sup> The temperature dependence of the AIGL growth rates is very small compared with the temperature dependence observed for the AEG film grown with TMA and EG. The temperature-independent growth of AIGL is attributed to extensive crosslinking that inhibits the TMA diffusion into the growing film that usually occurs during AEG MLD.<sup>[22]</sup>

One challenge exists for the alucone MLD process when using simple homobifunctional precursors such as EG. The homobifunctional precursors can react twice with the  $\text{AlCH}_3^*$  species. These “double reactions” reduce the number of hydroxyl groups that are available for reaction and lead to a decreased growth rate. A three-step ABC MLD cycle using three precursors has been used to circumvent the double-reaction problem.<sup>[42,43]</sup> Two heterobifunctional precursors, ethanolamine and maleic anhydride, are dosed sequentially after the TMA dose. Using the three-step MLD process avoids double reactions on both ends of the precursor molecular and leads to continuous growth of the alucone film. In addition to using the three-step MLD process, heterobifunctional precursors, such as glycidol, have been used for alucone film growth.<sup>[44,45]</sup> Based on the reaction selectivity of  $\text{AlCH}_3^*$  with OH and epoxy groups, glycidol can minimize double reactions, leading to relatively stable hybrid organic-inorganic films.<sup>[45]</sup>

An alternative approach to avoid double reactions is to introduce aromatic organic diols with a rigid structure. For example, the organic diol, hydroquinone (HQ), and TMA can be used in a sequential reaction procedure shown in Figure 4a. Polymer chains with the form of  $(-\text{O}-\text{C}_6\text{H}_4-\text{O}-\text{Al}-)_n$  comprise the alucone AlHQ MLD film.<sup>[46]</sup> The AlHQ film forms electronically conductive structures.<sup>[5,47]</sup> Further dehydrogenation occurs when annealing the as-deposited film under both inert and air atmosphere as shown in Figure 4b. Dehydrogenation induces a longitudinal crosslinking reaction of the aluminum-dioxybenzene chains. The three-dimensional (3-D) crosslinked structure leads to improved conductive and mechanical properties.<sup>[5]</sup>

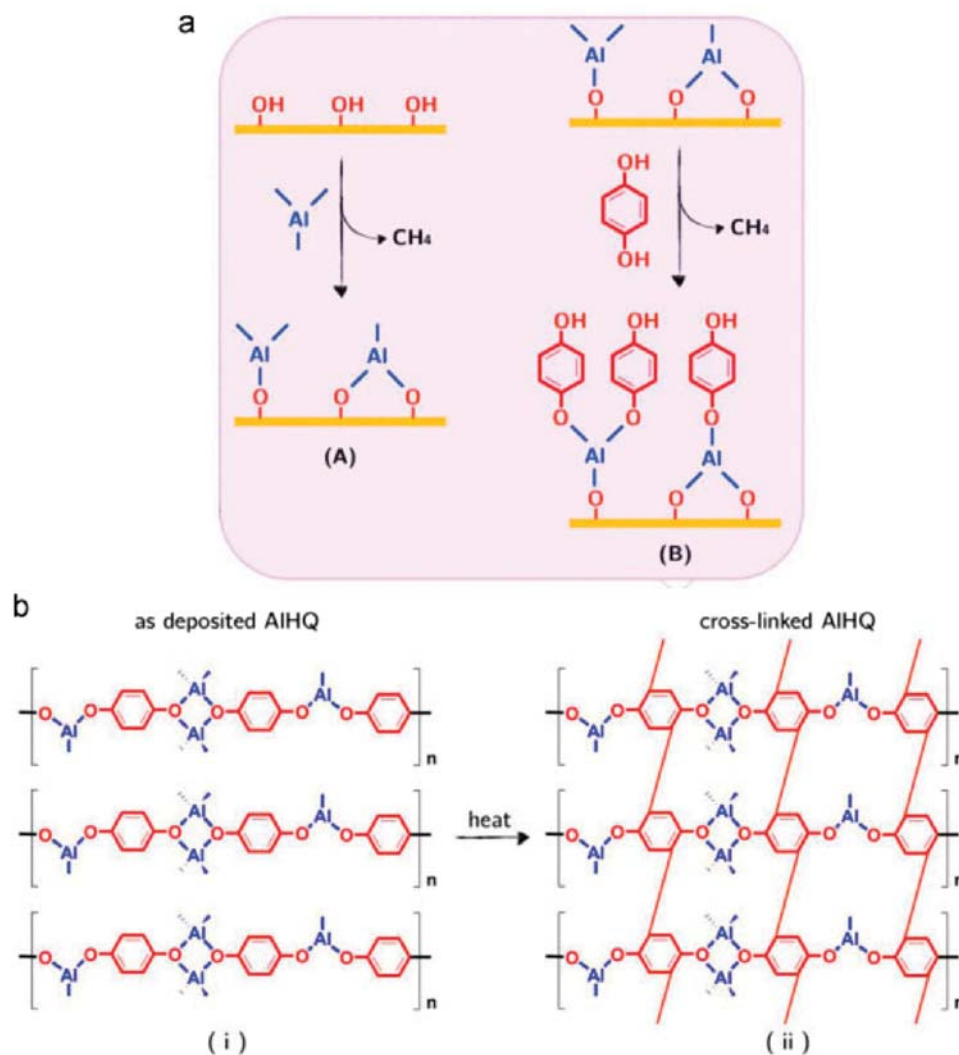
The MLD of hybrid organic-inorganic polymers can also be combined with ALD of inorganic materials to form MLD/ALD alloys.<sup>[24,25]</sup> These MLD/ALD alloys are important because the relative amounts of MLD and ALD can be varied to tune the properties of the MLD/ALD alloy films.<sup>[24,25]</sup> Many properties of the MLD/ALD alloys can be tuned including the mechanical, optical, chemical and thermal properties.<sup>[24,25,33]</sup> The tuning of the mechanical properties may be very important to form flexible coatings for high-volume-expansion Si anodes.

Figure 5 shows the elastic modulus and hardness of MLD/ALD alloys deposited using alucone AIEG MLD with TMA and EG as the reactants and  $\text{Al}_2\text{O}_3$  ALD with TMA and  $\text{H}_2\text{O}$  as the reactants.<sup>[25]</sup> The composition of the MLD/ALD alloys was tuned by varying the relative number of MLD and ALD cycles used to grow the film. Figure 5a shows that the elastic modulus is very low at  $E = 21$  GPa for the pure alucone MLD films.<sup>[25]</sup> The elastic modulus then increases progressively as more ALD cycles are used to grow the MLD/ALD alloy film. The elastic modulus reaches a much higher value of  $E = 198$  GPa for the pure  $\text{Al}_2\text{O}_3$  ALD films.<sup>[25]</sup> A similar trend is observed for the hardness of the MLD/ALD alloys displayed in Figure 5b. The upper and lower bounds on the elastic modulus and hardness are the values predicted by a “rule of mixtures” estimation.<sup>[25]</sup> Analogous results were also observed for MLD/ALD alloys deposited using zircon MLD with zirconium tert-butoxide (ZTB) and EG as the reactants and  $\text{ZrO}_2$  ALD with ZTB and  $\text{H}_2\text{O}$  as the reactants.<sup>[24,39]</sup>

### 2.3. Liquid-Phase MLD

The low vapor pressure of MLD precursors often limits their application. Elevated temperatures have been applied to enhance the vapor pressure and reactivity of MLD precursors. However, the MLD precursor can also decompose at high temperatures. To avoid these problems, liquid-phase MLD can be employed as an alternative method to grow organic tailored materials.<sup>[48]</sup>

An illustration of the liquid-phase MLD procedure is displayed in Figure 6. After the reaction between surface species and molecule A, the reaction reaches its limiting value and new functional groups are present on the surface. Excess molecule A is then rinsed away. This rinsing functions similarly to the purging step in the gas-phase MLD sequence. Molecule B is then introduced to react with the reactive surface species provided by molecule A. The next reaction could then be with molecule A or with other reactants, such as molecules C and D,



**Figure 4.** (a) Schematic illustration of the surface chemistry during AIHQ MLD based on the sequential reactions of trimethylaluminum (Al(CH<sub>3</sub>)<sub>3</sub>) and hydroquinone (C<sub>6</sub>H<sub>4</sub>(OH)<sub>2</sub>). (b) Crosslinking of the AIHQ chains resulting from heat treatments. Dehydrogenation occurs during the annealing process and induces a longitudinal crosslinking of the aluminum-dioxybenzene chains. Reproduced with permission.<sup>[5]</sup> Copyright 2016, Elsevier.

as shown in Figure 6. This strategy enables the growth of various organic and hybrid organic-inorganic materials via liquid-phase sequential self-limiting reactions. Liquid-phase MLD can potentially modify the surface of Li-ion battery electrodes or be used for other applications such as coating particles for drug delivery.<sup>[49]</sup>

### 3. Unique Properties of MLD Coatings for Li-Ion Electrodes

One major problem that causes performance degradation in Li-ion batteries is parasitic reactions between organic electrolytes and the surface of electrode materials. These reactions result in large irreversible capacity loss, formation of solid electrolyte interphases (SEIs), and gradual electrolyte consumption during the electrode operation.<sup>[50,51]</sup> Another major problem is volume changes for high-capacity electrodes during cycling.

These volume changes result in cracking of the active material, and the loss of electronic connectivity and mechanical integrity in the composite electrode.<sup>[19,52]</sup>

Progress toward deploying the high-capacity Li-ion electrodes has been achieved by introducing various functional coatings.<sup>[7,53–56]</sup> The functional coatings can enhance the stability of the electrodes after chemically interacting with electrolytes. The coatings can also accommodate volume fluctuations for the high-capacity anodes that have corresponding high volume changes. In addition, the coatings can also improve the conductivity for the systems that require high-rate performance. Conductive carbon coating has been used extensively to improve cycling capacity, particularly during rapid charge and discharge.<sup>[55–57]</sup>

Significantly improved cycling performance has also been demonstrated for both layered metal-oxide cathodes and graphite anodes coated with insulating coatings, such as Al<sub>2</sub>O<sub>3</sub> and ZrO<sub>2</sub>.<sup>[10,58–61]</sup> Unfortunately, the Al<sub>2</sub>O<sub>3</sub> coating has little

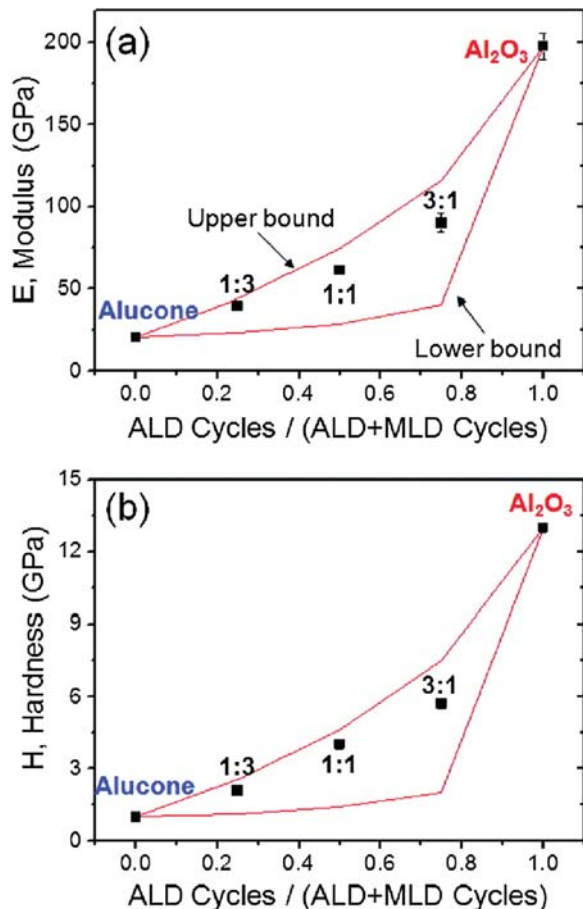


**Figure 5.** Elastic modulus (a) and hardness (b) versus fraction of ALD cycles used during the growth of the alucone alloy films. The alucone alloy film is deposited with alucone MLD using TMA and EG as the reactants and Al<sub>2</sub>O<sub>3</sub> ALD with TMA and H<sub>2</sub>O as the reactants. Reproduced with permission.<sup>[25]</sup> Copyright 2012, American Chemical Society.

impact on the cycling performance of Si anodes.<sup>[62]</sup> The explanation of the mixed results for Li metal oxide cathodes, graphite anodes and Si anodes is that one or two coating materials can not meet the diverse requirements of different electrodes.

Basically, there is no universal coating material that can satisfy all Li-ion electrodes.

Previous reviews have focused on the effect of ALD metal oxide coatings on Li-ion battery performance.<sup>[26]</sup> In contrast, this review summarizes recent results using MLD as a new technique to modify high-capacity electrodes that display large volumetric changes. Table 1 lists the MLD coating materials that have shown a significant impact on stabilizing the cycling performance of these high-capacity electrodes. The following sections describe the major features of the MLD coatings that have been utilized to improve the cycling performance of Li-ion electrodes.

### 3.1. Covalent-Bonding Enhanced Adhesion

One important feature of the ALD and MLD techniques is the capability to provide covalently bonded coatings to the electrode surfaces. The failure of Si composite electrodes is partially attributed to the poor adhesion between the coating and the electrode. The adhesion must be strong to prevent the failure at the interface and also to maintain mechanical integrity during volume changes. Based on the alloying/dealloying reactions, Si-based electrodes experience about 370%–400% volume expansion during lithiation and corresponding contraction during delithiation,<sup>[63]</sup> which causes much more drastic, three-dimensional structural rearrangements.

Figure 7 shows the TEM micrographs of a Si electrode, made of Si active materials, acetylene black, and polyvinylidene difluoride (PVDF).<sup>[6]</sup> After 20 cycles of lithiation and delithiation, the separation is clearly observed between the Si particles and PVDF matrix. The weak binding between PVDF and Si particles causes cracking in the composite electrode and the isolation of active material from the electrical matrix. This cracking and isolation contributes to rapid capacity degradation.

The introduction of covalently bonded organic-inorganic coating on the surface of Si particles significantly improves the adhesion between the electrode and the coating. Using the ALGL MLD coating as an example, the first reaction between the TMA precursor and surface silanol groups of the native oxide can be written as:

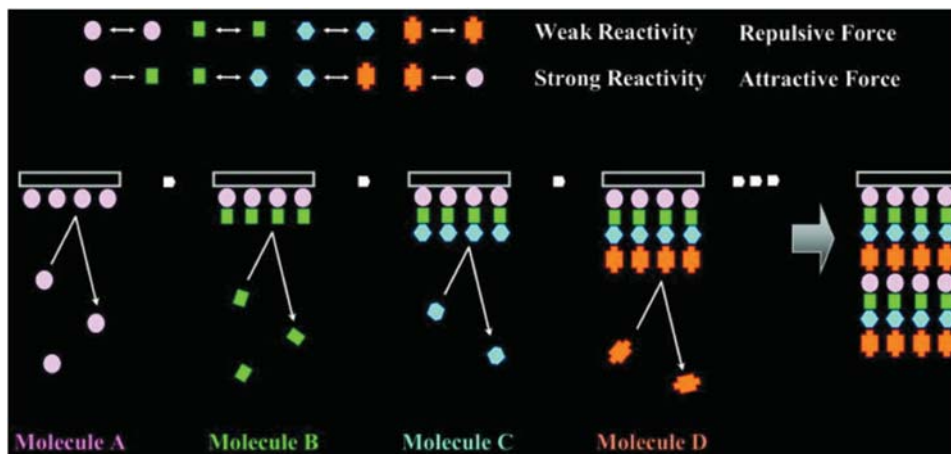


**Figure 6.** Schematic illustration of liquid-phase molecular layer deposition. Reproduced with permission.<sup>[48]</sup> Copyright 2011, Electrochemical Society.

**Table 1.** MLD coatings for surface modification of Li-ion electrodes.

Coating materials	MLD reactants	Function	Coating effect	Ref.
Aluminum glycerol	TMA, GLY	Surface modification for Si anodes	Accommodate the volumetric changes, mitigate the surface side reactions and improve the cycling performance	[6]
Aluminum hydroquinone	TMA, HQ	Surface modification for Si anode	Accommodate the volumetric changes, mitigate the surface side reactions and improve the cycling performance	[5]
Aluminum ethylene glycol	TMA, EG	Surface modification for sulfur electrodes	Suppress the dissolution of poly sulfide anions, improve cycling performance	[71,72]



or



The calculated reaction energies of  $-1.86$  eV and  $-3.00$  eV for the reactions given by Equations (3) and (4), respectively, indicate that these thermodynamically favorable reactions can establish chemical bonds between coatings such as the ALGL film and the Si surface.<sup>[64]</sup> Subsequently, the  $\text{AlCH}_3^*$  surface species can have energetically favorable reaction with diols or triols, such as ethylene glycol, glycerol, and hydroquinone, to form polymeric 3D structures. Based on simulation results, the polymeric coating via MLD is packed very tightly with many crosslinks and branch chains.<sup>[64]</sup> The covalent layer-by-layer process of assembling the film provides intimate adherence between the Si nanoparticles and the polymeric coating.

The TEM images in **Figure 8** record lithium insertion in the alucone ALGL-coated Si particles at 0, 21, 58, and 81 s.<sup>[65]</sup> Lithiation starts from the alucone layer and gradually proceeds inward, leading to the formation of a layered configuration including ALGL coating, amorphous Si, and the crystalline unreacted Si. This intimate contact between particle and coating provides mechanical strength that maintains the original electrode network, prevents the isolation of active material, and enables its full utilization throughout cycling. Most importantly, the swelling of the alucone ALGL coating along with lithiation helps the alucone ALGL coating to expand with the Si particle. Upon delithiation, the coated Si particles together with the ALGL coating will contract without pore formation or coating delamination.<sup>[65]</sup>

### 3.2. Elasticity of MLD Coatings to Accommodate Volumetric Changes

Elasticity is essential for coatings on high-capacity Li-ion electrodes that exhibit huge volumetric changes. When Si-based alloys and sulfur-based materials are used as electrodes, rigid inorganic ALD coatings have a limited ability to accommodate the large volume change during charging and discharging. Fortunately, there are many organic and hybrid organic-inorganic films that have been grown using MLD techniques. The flexibility of these films can be measured by their Young's modulus of elasticity and hardness. The mechanical properties of various alucones obtained by nanoindentation measurements are summarized in **Table 2**. Much lower Young's moduli of elasticity are observed in these MLD coatings compared with ALD coatings. The Young's modulus for alucone ALGL is 32.0 GPa.<sup>[6,41]</sup> In comparison, the Young's modulus for  $\text{Al}_2\text{O}_3$  ALD films has been measured to be 198 GPa,<sup>[25]</sup> 220 GPa,<sup>[66]</sup> 168–182 GPa,<sup>[67]</sup> and 195–203 GPa.<sup>[68]</sup>

The wear resistance is another parameter that determines the mechanical performance of a coating material. The ratio of hardness to Young's modulus (H/E) determines the wear resistance of the film.<sup>[69,70]</sup> A higher H/E ratio suggests a more elastic than plastic deformation under external force. Materials with higher H/E ratios are expected to have smaller accumulative strains and strain energies. These materials should also have better wear resistance and higher durability under severe mechanical loading.<sup>[69,70]</sup> The MLD films in Table 2 have H/E ratios between  $1.3\text{--}8.3 \times 10^{-2}$ . The hardness for  $\text{Al}_2\text{O}_3$  ALD films has been measured to be 13.0 GPa,<sup>[25]</sup> 10.5 GPa,<sup>[66]</sup> 12.3 GPa, and 6.7 GPa.<sup>[68]</sup> Using a Young's modulus of  $\approx 200$  GPa, the H/E ratios for the  $\text{Al}_2\text{O}_3$  ALD films from these hardness measurements are between  $3.4\text{--}6.5 \times 10^{-2}$ . The  $\text{Al}_2\text{O}_3$

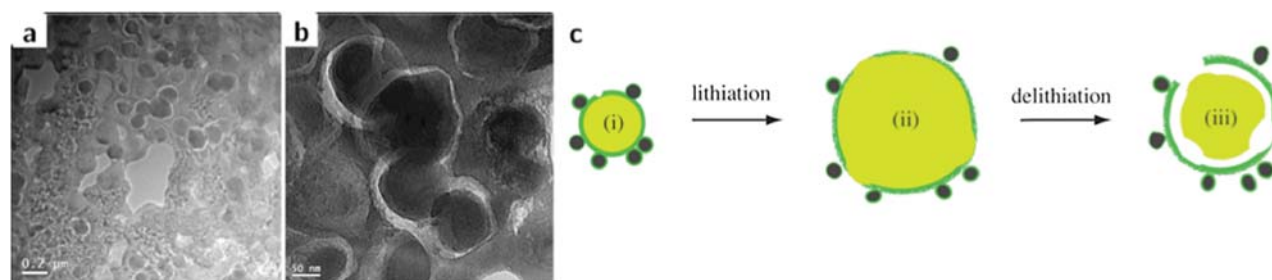


**Figure 7.** (a), (b) TEM images of the nano-silicon electrode after 20 electrochemical cycles. The electrode shows the separation between the nano-Si particles and the electrode network. This separation isolates active material from the conductive matrix and causes rapid capacity degradation. (c) Schematic illustration of the lithiation-delithiation mechanism in the nano-silicon electrode. Reproduced with permission.<sup>[6]</sup>

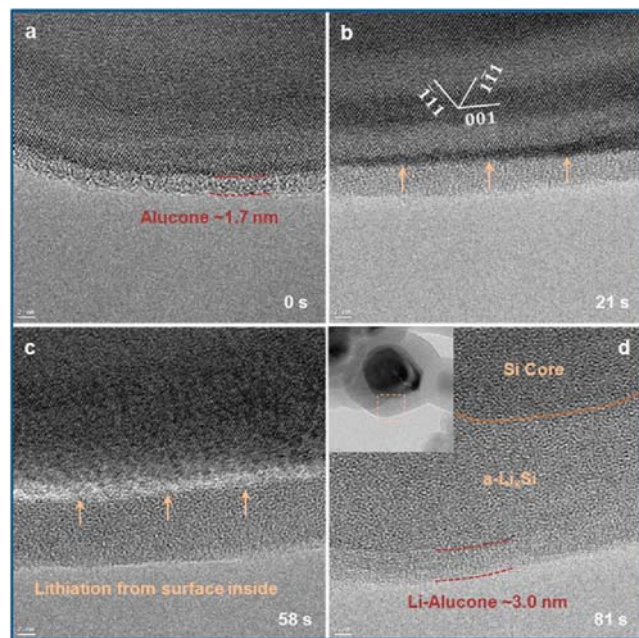


**Figure 8.** High-resolution TEM images recorded during in situ TEM observation revealing details of the lithiation process in the alucone-coated Si nanoparticle. Arrows indicate reaction front. Reproduced with permission.<sup>[65]</sup> Copyright 2014, American Chemical Society.

ALD coatings have similar H/E ratios compared with the alucone MLD coatings.

The impact of Al<sub>2</sub>O<sub>3</sub> ALD and alucone MLD coatings on electrochemical cycling behavior has been demonstrated by studies of Al<sub>2</sub>O<sub>3</sub> ALD and alucone MLD-coated Si anodes. PVDF was used in the study to distinguish the impact of the alucone coating from the effect of polymer binders. Results for the specific capacity versus cycle number for uncoated, Al<sub>2</sub>O<sub>3</sub> ALD, ALGL alucone MLD and ALHQ alucone MLD-coated Si anodes are displayed in **Figure 9**. The results from the Al<sub>2</sub>O<sub>3</sub> ALD-coated Si anodes shown in Figure 9a indicate that the rigid Al<sub>2</sub>O<sub>3</sub> ALD coating failed and led to fast capacity fade. In contrast, the ALGL-coated Si electrode exhibits significant cycling stability as shown in Figure 9b.<sup>[6]</sup> There is a specific capacity of nearly 900 mAh g<sup>-1</sup> at cycle 150. In comparison, the uncoated Si electrode undergoes rapid capacity decay caused by surface side reactions and mechanical failure. The uncoated Si electrodes have negligible specific capacity after 35 cycles.

Further improvement has been achieved when using a crosslinked ALHQ alucone MLD coating. These results are

displayed in Figure 9c.<sup>[5]</sup> The ALHQ-coated Si electrode after 200 °C annealing delivers a higher capacity than the ALHQ-coated Si electrode prior to annealing. The improved conductivity from the crosslinked aromatic backbone is believed to facilitate the charge transport. This higher conductivity leads to a higher capacity than the capacity of other coated electrodes.<sup>[5]</sup>

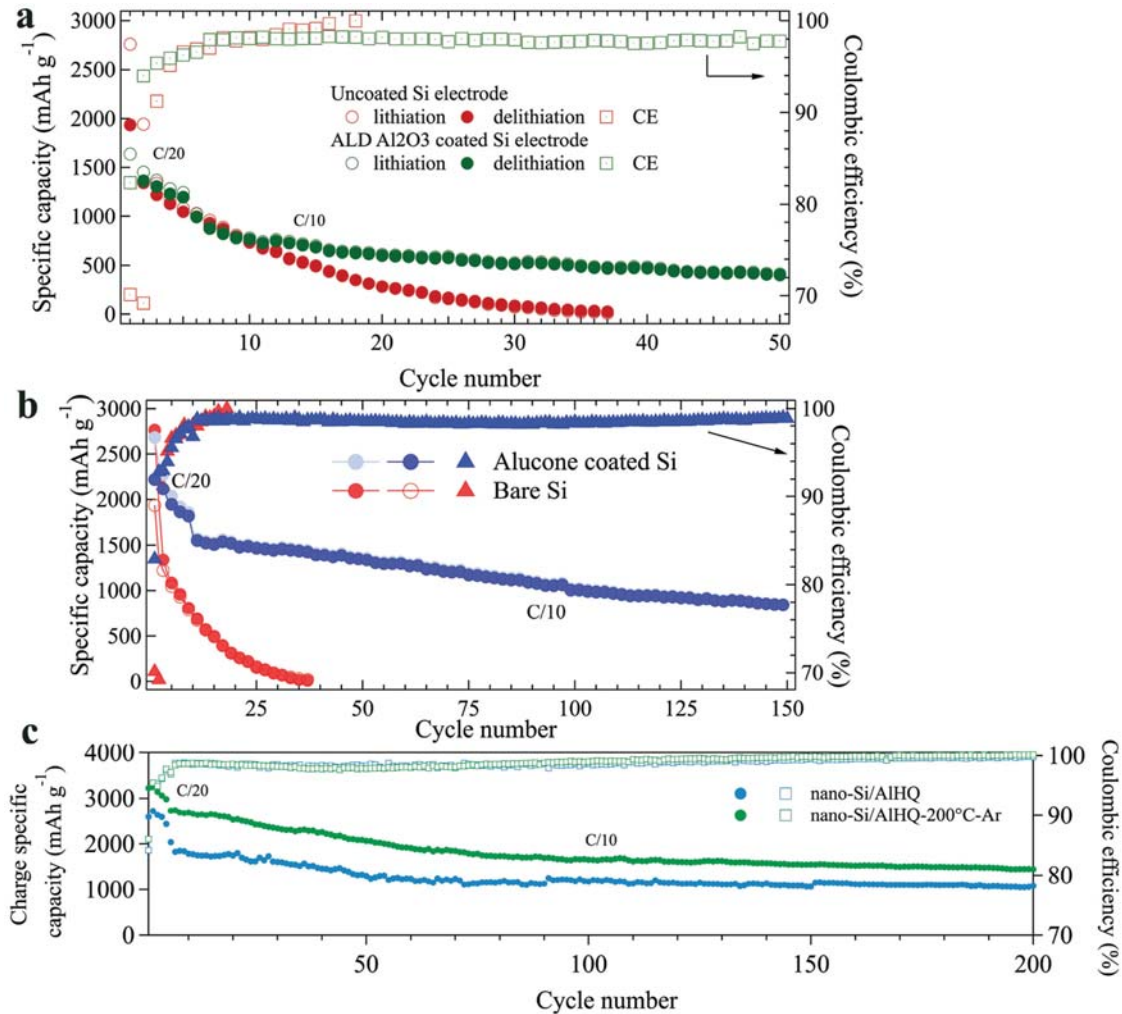
The Coulombic efficiency (CE) is the ratio between the capacity at delithiation and capacity at lithiation. CE corresponds to the reversibility of the lithiation/delithiation reactions. The first-cycle CE for the uncoated Si electrode is low at ~68%. In addition to the side reactions at the Si electrode surfaces, three-dimensional structural rearrangement causes loss of electrical conduction pathways and leads to the low CE for the first cycle. By using MLD coatings, the CEs in all of the coated Si electrodes improved to ≥84% as shown in Figures 9b and 9c. The improved CE and capacity stability is evidence that the elastic ALGL coatings not only chemically modify the surface, but also provide favorable mechanical properties to enhance the structural stability of the Si electrodes.

High-energy sulfur (S) cathode materials need coatings to prevent the dissolution of polysulfides, accommodate volume expansion, and maintain the conductive network. Sulfur cathodes must also overcome the severe challenges of their insulating nature and polysulfide dissolution in organic electrolyte. An ultrathin alucone ALEG coating has been applied on a carbon-sulfur (C-S) composite electrode.<sup>[71,72]</sup> The coating stabilized the cycling performance with improvements in capacity retention, utilization of active material, and rate capability. Results for the cycle performance for bare, Al<sub>2</sub>O<sub>3</sub> ALD-coated and alucone MLD-coated cathodes are shown in **Figure 10**.<sup>[71]</sup> The best performance was observed for the alucone MLD-coated cathodes. The ultrathin ALEG coating layer was believed to restrain the dissolution of polysulfides while keeping the electrical network stable against volume changes of S active materials.

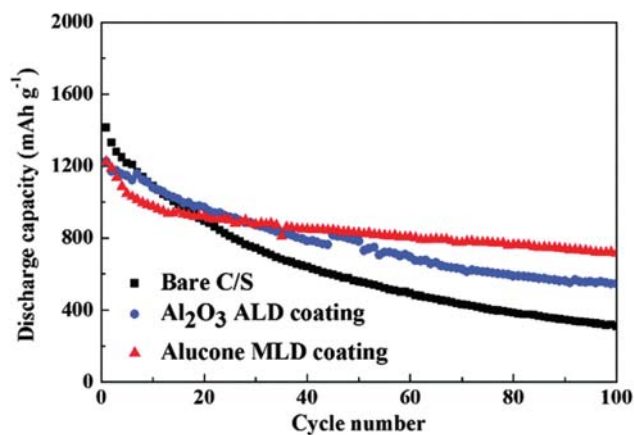
The ALEG coating is known to serve as an interlayer to minimize stress between two films with expansion mismatch. Previous studies have examined the ability of ALEG interlayers to minimize stress between Al<sub>2</sub>O<sub>3</sub> ALD films and Teflon fluorinated ethylene propylene (FEP) substrates.<sup>[73]</sup> The large mismatch of thermal-expansion coefficient between the Teflon FEP substrate and Al<sub>2</sub>O<sub>3</sub> ALD films caused large compressive stresses on the Al<sub>2</sub>O<sub>3</sub> ALD film when the Teflon FEP substrate was cooled to room temperature after deposition of the Al<sub>2</sub>O<sub>3</sub> ALD film at elevated temperatures.<sup>[73]</sup> This compressive stress could buckle and crack the Al<sub>2</sub>O<sub>3</sub> ALD film. The ALEG interlayer minimized the compressive strain and lowered the crack density in the Al<sub>2</sub>O<sub>3</sub> ALD film.

**Table 2.** Mechanical properties of alucones grown using TMA and different diols and triols.

Coating Materials	Reactants	Growth Rate (Å/MLD cycle)	Density (g/cm <sup>3</sup> )	Young's Modulus (GPa)	Hardness (GPa)	H/E (×100)	Ref.
Alucone	TMA, EG	0.4 (175 °C)	1.5	36.8	0.47	1.3	[25,76]
Alucone	TMA, GL	2.5 (140 °C)	1.6	32.0	2.66	8.3	[6,41]
Alucone	TMA, GLY	1.3 (125 °C)	1.6				[45]
Alucone	TMA, HQ	7.5 (150 °C)	1.6	29.2	1.24	4.2	[5]
Alucone, annealed at 150 °C	TMA, HQ		1.7	34.9	1.82	5.2	[5]
Alucone, annealed at 200 °C	TMA, HQ		1.7	60.2	2.50	4.2	[5]

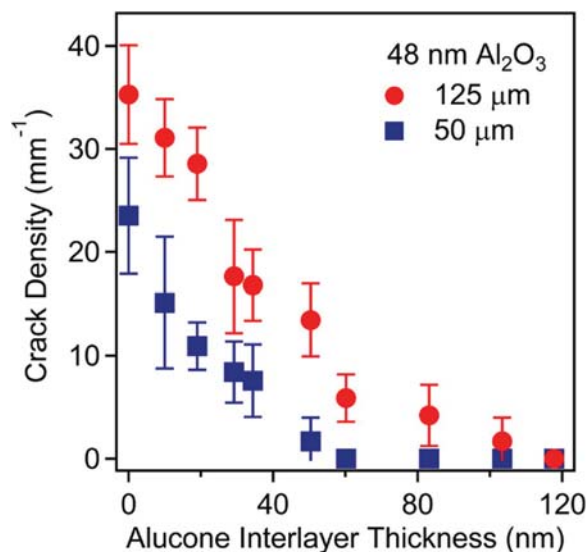


**Figure 9.** (a) Cycling performance of ALD Al<sub>2</sub>O<sub>3</sub>-coated Si anode in comparison with the cycling behavior of the uncoated Si electrode. (b) Cyclic capacity and CE of the ALGL-coated Si anode in comparison with the capacity and CE of the uncoated Si electrode. Reproduced with permission.<sup>[6]</sup> (c) Cyclic capacity and CE of the silicon anode coated with AIHQ compared with the cyclic capacity and CE of the Si anode coated with AIHQ after annealing. Reproduced with permission.<sup>[5]</sup> Copyright 2016, Elsevier.



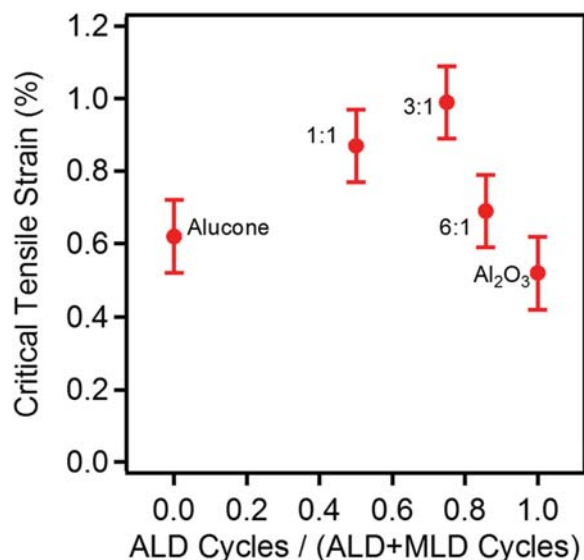
**Figure 10.** Comparison of cycle performances for uncoated, Al<sub>2</sub>O<sub>3</sub> ALD-coated, and alucone MLD-coated sulfur cathodes at a current density of 160 mA g<sup>-1</sup>. Reproduced with permission.<sup>[71]</sup> Copyright 2014, Royal Society of Chemistry.

Figure 11 shows the crack density in an Al<sub>2</sub>O<sub>3</sub> ALD film with a thickness of 48 nm versus the alucone interlayer thickness for Teflon FEP substrates with thicknesses of 50 and 120 μm.<sup>[73]</sup> The Al<sub>2</sub>O<sub>3</sub> ALD and alucone MLD films were grown at 135 °C and then cooled to room temperature. The crack density was determined from the number of cracks along the direction of the tensile strain over a length of 90 μm. The alucone interlayers dramatically reduced the crack density in the Al<sub>2</sub>O<sub>3</sub> ALD film. No cracks were observed in the Al<sub>2</sub>O<sub>3</sub> ALD film when the thickness of the alucone interlayer was above 50 nm for the 50 μm Teflon FEP substrates. Thinner alucone MLD films can reduce the crack density on the thinner Teflon FEP substrates and thinner Al<sub>2</sub>O<sub>3</sub> ALD films. The alucone MLD film was believed to serve as a “bed of springs” to minimize the compressive stress on the Al<sub>2</sub>O<sub>3</sub> ALD film.<sup>[73]</sup> The “spring-like” nature of the alucone MLD film may also help to accommodate the stresses caused by volume expansion and contraction and mitigate the expansion mismatch between bulk Si particles and SEI films during the lithiation and delithiation of high-capacity electrodes.



**Figure 11.** Cracking density of Al<sub>2</sub>O<sub>3</sub> ALD films with a thickness of 48 nm vs. the alucone interlayer thickness for Teflon FEP substrates with thicknesses of 50 and 125 μm. Reproduced with permission.<sup>[73]</sup> Copyright 2013, American Chemical Society.

Additional measurements of the critical tensile strain of MLD/ALD nanolaminates were performed using alucone MLD with TMA and EG as the reactants and Al<sub>2</sub>O<sub>3</sub> ALD using TMA and H<sub>2</sub>O as the reactants.<sup>[74]</sup> These studies revealed that the MLD/ALD nanolaminates had a higher critical tensile strain than either the pure alucone MLD film or Al<sub>2</sub>O<sub>3</sub> ALD film. The critical tensile strain for the MLD/ALD nanolaminates is shown in Figure 12.<sup>[74]</sup> The nanolaminates were grown by varying the number of ALD cycles and MLD cycles used for one bilayer in the nanolaminate. Compared with the pure alucone MLD film or Al<sub>2</sub>O<sub>3</sub> ALD film, the critical tensile strain increased ≈50% for



**Figure 12.** Critical tensile strain for alucone MLD/Al<sub>2</sub>O<sub>3</sub> ALD nanolaminates with a thickness of ≈100 nm. The critical tensile strains are plotted versus the fraction of Al<sub>2</sub>O<sub>3</sub> ALD cycles in the reaction sequence. Reproduced with permission.<sup>[74]</sup> Copyright 2012, AIP Publishing LLC.

the 3:1 ALD:MLD film. These MLD/ALD nanolaminate films may also be useful to respond to the stresses caused by the large-volume-change transformations during the operation of high-capacity electrodes.

### 3.3. Stability and Interaction with Organic Li-Ion Electrolytes

The first alucone MLD film was successfully fabricated using TMA and EG as the reactants.<sup>[22]</sup> However, a 20% loss of film thickness was observed after aging at ambient environment.<sup>[22]</sup> Other researchers confirmed the instability of the ALEG film. They attributed the instability to the exposure of water.<sup>[75]</sup> A C=C vibrational feature appeared when comparing the FTIR spectra collected from the ALEG MLD film that was stored in air for 2 months with the as-grown ALEG MLD film. The formation of CH<sub>2</sub>=CH-O-Al and HO-CH=CH-O-Al structures is believed to coincide with the reactions with water.<sup>[22]</sup>

The stability to water exposures has been greatly improved when using other organic precursors besides EG. For example, FTIR spectroscopy was applied to investigate the stability of AlGLY, the alucone film grown with glycidol.<sup>[44]</sup> The absence of any new C=C vibrational features corresponds with stable thickness after long exposures to the ambient air.<sup>[44]</sup> Further investigation of the thermal stability confirmed that the AlGLY film was stable in air at 100 °C. Dehydration occurred when the film was annealed at 200 °C. Decomposition began at 300 °C. Improved stability was also achieved using other precursors including GL and HQ. The higher stability was attributed to the more complete precursor reactivity and the formation of crosslinking structure.<sup>[41,47]</sup>

The reactivity of AlGL with the carbonate organic electrolyte was also studied using DFT, *ab initio* molecular dynamics (AIMD), and DFT-Green's function analysis.<sup>[64]</sup> The results suggested that lithium ions can be trapped in the AlGL film during the first lithiation process. The lithiated AlGL film then becomes electronically conductive.<sup>[64]</sup> Saturated AlGL film can facilitate lithium diffusion without consuming lithium ions. The calculated results are consistent with the experimental data and confirm the rapid lithiation process enabled by the AlGL coating.

## 4. Summary and Outlook

The need for high-energy-storage Li-ion batteries has motivated the development of high-capacity electrode materials that experience large volume changes during lithiation and delithiation. The alloying/dealloying or conversion reactions in these high-capacity electrode materials causes drastic, three-dimensional structural rearrangements. These rearrangements result in substantial volumetric changes, rapid disintegration, loss of electrical connection to the current collector, and finally, rapid degradation in cycling performance. Moreover, the inherent non-passivating behavior of silicon in organic electrolytes results in large irreversible capacity loss and gradual electrolyte consumption during electrode operation.

A successful surface coating for these high-capacity electrode materials must be electrochemically stable against electrolyte, mitigate parasitic reactions on the surface of the electrodes,

accommodate the volumetric changes and maintain the mechanical integrity. This review has focused on the relatively new method, MLD, and its unique features to develop covalently bonded hybrid coatings for porous three-dimensional electrode architectures. Based on self-limited and sequential reactions, MLD can realize the growth of ultrathin flexible films that conform to complex substrates with excellent control of composition and thickness.

The MLD films can be adjusted for particular chemical, electrical and mechanical properties by varying the MLD film composition and incorporating designed functionalities into the MLD process. In the future, the ability to tune the MLD film should lead to improved strategies for addressing degradation caused by mechanical failure and surface instability of Li-ion electrodes. Previous work has only examined the alucones with a small set of organic functional groups. Future work should explore other hybrid organic-inorganic MLD films and vary their chemical, electrical and mechanical properties. These efforts will continue to build our understanding of the interaction between the surface coating and organic electrolytes, and the relationship between the coating and its electrochemical and mechanical behavior. The result will be new functional coating materials designed for the needs of high-performance Li-ion batteries.

## Acknowledgements

Financial support is greatly appreciated from Energy Efficiency and Renewable Energy, Office of Vehicle Technologies, U.S. Department of Energy under Contract No. DE-AC-36-08GO28308 under the Applied Batteries Research (ABR) Program.

Received: August 4, 2016

Revised: August 29, 2016

Published online:

- [1] M. S. Whittingham, *Science* **1976**, *192*, 1126.
- [2] J. B. Goodenough, Y. Kim, *J. Power Sources* **2011**, *196*, 6688.
- [3] S. B. Son, B. Kappes, C. Ban, *Isr. J. Chem.* **2015**, *55*, 558.
- [4] K. Xu, *Chem. Rev.* **2014**, *114*, 11503.
- [5] D. M. Piper, Y. Lee, S.-B. Son, T. Evans, F. Lin, D. Nordlund, X. Xiao, S. M. George, S.-H. Lee, C. Ban, *Nano Energy* **2016**, *22*, 202.
- [6] D. M. Piper, J. J. Travis, M. Young, S.-B. Son, S. C. Kim, K. H. Oh, S. M. George, C. Ban, S.-H. Lee, *Adv. Mater.* **2014**, *26*, 1596.
- [7] D. M. Piper, T. A. Yersak, S.-B. Son, S. C. Kim, C. S. Kang, K. H. Oh, C. Ban, A. C. Dillon, S.-H. Lee, *Adv. Energy Mater.* **2013**, *3*, 697.
- [8] Y. S. Jung, A. S. Cavanagh, Y. Yan, S. M. George, A. Manthiram, *J. Electrochem. Soc.* **2011**, *158*, A1298.
- [9] Y. S. Jung, A. S. Cavanagh, L. A. Riley, S. H. Kang, A. C. Dillon, M. D. Groner, S. M. George, S. H. Lee, *Adv. Mater.* **2010**, *22*, 2172.
- [10] Y. S. Jung, P. Lu, A. S. Cavanagh, C. Ban, G.-H. Kim, S.-H. Lee, S. M. George, S. J. Harris, A. C. Dillon, *Adv. Energy Mater.* **2013**, *3*, 213.
- [11] S. M. George, *Chem. Rev.* **2010**, *110*, 111.
- [12] R. L. Puurunen, *J. Appl. Phys.* **2005**, *97*, 121301.
- [13] V. Miikkulainen, M. Leskela, M. Ritala, R. L. Puurunen, *J. Appl. Phys.* **2013**, *113*, 021301.
- [14] Y. S. Jung, A. S. Cavanagh, A. C. Dillon, M. D. Groner, S. M. George, S. H. Lee, *J. Electrochem. Soc.* **2010**, *157*, A75.
- [15] S. C. Lai, *J. Electrochem. Soc.* **1976**, *123*, 1196.
- [16] J. Graetz, C. C. Ahn, R. Yazami, B. Fultz, *Electrochem. Solid State Lett.* **2003**, *6*, A194.
- [17] C. K. Chan, H. Peng, G. Liu, K. McIlwrath, X. F. Zhang, R. A. Huggins, Y. Cui, *Nature Nanotech.* **2008**, *3*, 31.
- [18] X. H. Liu, L. Zhong, S. Huang, S. X. Mao, T. Zhu, J. Y. Huang, *ACS Nano* **2012**, *6*, 1522.
- [19] C.-M. Wang, X. Li, Z. Wang, W. Xu, J. Liu, F. Gao, L. Kovarik, J.-G. Zhang, J. Howe, D. J. Burton, Z. Liu, X. Xiao, S. Thevuthasan, D. R. Baer, *Nano Letters* **2012**, *12*, 1624.
- [20] M. T. McDowell, I. Ryu, S. W. Lee, C. Wang, W. D. Nix, Y. Cui, *Adv. Mater.* **2012**, *24*, 6034.
- [21] T. Yoshimura, S. Tatsuura, W. Sotoyama, *Appl. Phys. Lett.* **1991**, *59*, 482.
- [22] A. A. Dameron, D. Seghete, B. B. Burton, S. D. Davidson, A. S. Cavanagh, J. A. Bertrand, S. M. George, *Chem. Mater.* **2008**, *20*, 3315.
- [23] S. M. George, B. Yoon, A. A. Dameron, *Acc. Chem. Res.* **2009**, *42*, 498.
- [24] B. H. Lee, B. Yoon, A. I. Abdulagatov, R. A. Hall, S. M. George, *Adv. Funct. Mater.* **2013**, *23*, 532.
- [25] B. H. Lee, B. Yoon, V. R. Anderson, S. M. George, *J. Phys. Chem. C* **2012**, *116*, 3250.
- [26] X. Meng, X.-Q. Yang, X. Sun, *Adv. Mater.* **2012**, *24*, 3589.
- [27] T. Yoshimura, S. Tatsuura, W. Sotoyama, A. Matsuura, T. Hayano, *Appl. Phys. Lett.* **1992**, *60*, 268.
- [28] Y. Du, S. M. George, *J. Phys. Chem. C* **2007**, *111*, 8509.
- [29] N. M. Adamczyk, A. A. Dameron, S. M. George, *Langmuir* **2008**, *24*, 2081.
- [30] P. W. Loscutoff, H. B. R. Lee, S. F. Bent, *Chem. Mater.* **2010**, *22*, 5563.
- [31] T. V. Ivanova, P. S. Maydannik, D. C. Cameron, *J. Vac. Sci. Technol. A* **2012**, *30*.
- [32] H. Zhou, S. F. Bent, *J. Phys. Chem. C* **2013**, *117*, 19967.
- [33] P. Sundberg, M. Karppinen, *Beilstein J. Nanotechnol.* **2014**, *5*, 1104.
- [34] H. Zhou, S. F. Bent, *J. Vac. Sci. Technol. A* **2013**, *31*, 040801.
- [35] M. E. Alf, A. Asatekin, M. C. Barr, S. H. Baxamusa, H. Chelawat, G. Ozaydin-Ince, C. D. Petruczok, R. Sreenivasan, W. E. Tenhaeff, N. J. Trujillo, S. Vaddiraju, J. Xu, K. K. Gleason, *Adv. Mater.* **2010**, *22*, 1993.
- [36] S. M. George, B. H. Lee, B. Yoon, A. I. Abdulagatov, R. A. Hall, *J. Nanosci. Nanotechnol.* **2011**, *11*, 7948.
- [37] B. Yoon, J. L. O'Patches, D. Seghete, A. S. Cavanagh, S. M. George, *Chem. Vapor Deposition* **2009**, *15*, 112.
- [38] A. I. Abdulagatov, R. A. Hall, J. L. Sutherland, B. H. Lee, A. S. Cavanagh, S. M. George, *Chem. Mater.* **2012**, *24*, 2854.
- [39] B. H. Lee, V. R. Anderson, S. M. George, *Chem. Vapor Deposition* **2013**, *19*, 204.
- [40] B. H. Lee, V. R. Anderson, S. M. George, *ACS Appl. Mater. Interfaces* **2014**, *6*, 16880.
- [41] R. A. Hall, *Ph.D. Dissertation*, University of Colorado at Boulder, July 2013.
- [42] D. Seghete, R. A. Hall, B. Yoon, S. M. George, *Langmuir* **2010**, *26*, 19045.
- [43] B. Yoon, D. Seghete, A. S. Cavanagh, S. M. George, *Chem. Mater.* **2009**, *21*, 5365.
- [44] B. Gong, Q. Peng, G. N. Parsons, *J. Phys. Chem. B* **2011**, *115*, 5930.
- [45] Y. Lee, B. Yoon, A. S. Cavanagh, S. M. George, *Langmuir* **2011**, *27*, 15155.
- [46] B. Yoon, Y. Lee, A. Derk, C. B. Musgrave, S. M. George, *Electrochemistry of Novel Materials for Energy Storage and Conversion – 218th ECS Meeting*, Las Vegas, NV, **2011**; p 191.
- [47] D. Choudhury, S. K. Sarkar, N. Mahuli, *J. Vac. Sci. Technol. A* **2015**, *33*, 01A115.
- [48] T. Yoshimura, H. Watanabe, C. Yoshino, *J. Electrochem. Soc.* **2011**, *158*, P51.

- [49] T. Yoshimura, *Macromol. Sympos.* **2016**, 361, 141.
- [50] X. Su, Q. Wu, J. Li, X. Xiao, A. Lott, W. Lu, B. W. Sheldon, J. Wu, *Adv. Energy Mater.* **2014**, 4, 1300882.
- [51] M. T. McDowell, S. W. Lee, W. D. Nix, Y. Cui, *Adv. Mater.* **2013**, 25, 4966.
- [52] N. Yuca, H. Zhao, X. Song, M. F. Dogdu, W. Yuan, Y. Fu, V. S. Battaglia, X. Xiao, G. Liu, *ACS Appl. Mater. Interfaces* **2014**, 6, 17111.
- [53] I. Kim, P. N. Kumta, G. E. Blomgren, *Electrochem. Solid State Lett.* **2000**, 3, 493.
- [54] X. Q. Yang, J. McBreen, W. S. Yoon, M. Yoshio, H. Y. Wang, K. Fukuda, T. Umeno, *Electrochem. Comm.* **2002**, 4, 893.
- [55] R. Yi, F. Dai, M. L. Gordin, H. Sohn, D. Wang, *Adv. Energy Mater.* **2013**, 3, 1507.
- [56] R. C. de Guzman, J. H. Yang, M. M. C. Cheng, S. O. Salley, K. Y. S. Ng, *J. Power Sources* **2014**, 246, 335.
- [57] T. D. Bogart, D. Oka, X. Lu, M. Gu, C. Wang, B. A. Korgel, *ACS Nano* **2014**, 8, 915.
- [58] Y. S. Jung, A. S. Cavanagh, L. Gedvilas, N. E. Widjonarko, I. D. Scott, S. H. Lee, G. H. Kim, S. M. George, A. C. Dillon, *Adv. Energy Mater.* **2012**, 2, 1022.
- [59] J. Z. Kong, S. S. Wang, G. A. Tai, L. Zhu, L. G. Wang, H. F. Zhai, D. Wu, A. D. Li, H. Li, *J. Alloys Compd* **2016**, 657, 593.
- [60] J. Liu, X. Li, M. Cai, R. Li, X. Sun, *Electrochim Acta* **2013**, 93, 195.
- [61] J. Zhao, Y. Wang, *Nano Energy* **2013**, 2, 882.
- [62] L. Luo, H. Yang, P. Yan, J. J. Travis, Y. Lee, N. Liu, D. Molina Piper, S.-H. Lee, P. Zhao, S. M. George, J.-G. Zhang, Y. Cui, S. Zhang, C. Ban, C.-M. Wang, *ACS Nano* **2015**, 9, 5559.
- [63] M. N. Obrovac, L. Christensen, *Electrochem. Solid State Lett.* **2004**, 7, A93.
- [64] Y. Ma, J. M. Martinez De La Hoz, I. Angarita, J. M. Berrio-Sanchez, L. Benitez, J. M. Seminario, S. B. Son, S. H. Lee, S. M. George, C. Ban, P. B. Balbuena, *ACS Appl. Mater. Interfaces* **2015**, 7, 11948.
- [65] Y. He, D. M. Piper, M. Gu, J. J. Travis, S. M. George, S. H. Lee, A. Genc, L. Pullan, J. Liu, S. X. Mao, J. G. Zhang, C. M. Ban, C. M. Wang, *ACS Nano* **2014**, 8, 11816.
- [66] K. Tapily, J. E. Jakes, D. S. Stone, P. Shrestha, D. Gu, H. Baumgart, A. A. Elmustafa, *J. Electrochem. Soc.* **2008**, 155, H545.
- [67] M. K. Tripp, C. Stampfer, D. C. Miller, T. Helbling, C. F. Hermann, C. Hierold, K. Gall, S. M. George, V. M. Bright, *Sensor. Actuat. A-Phys.* **2006**, 130, 419.
- [68] D. C. Miller, R. R. Foster, S. H. Jen, J. A. Bertrand, S. J. Cunningham, A. S. Morris, Y. C. Lee, S. M. George, M. L. Dunn, *Sensor. Actuat. A-Phys.* **2010**, 164, 58.
- [69] Y.-T. Cheng, C.-M. Cheng, *Mater. Sci. Eng. R* **2004**, 44, 91.
- [70] A. Leyland, A. Matthews, *Wear* **2000**, 246, 1.
- [71] X. Li, A. Lushington, J. Liu, R. Li, X. Sun, *Chem. Commun.* **2014**, 50, 9757.
- [72] X. Li, A. Lushington, Q. Sun, W. Xiao, J. Liu, B. G. Wang, Y. F. Ye, K. Q. Nie, Y. F. Hu, Q. F. Xiao, R. Y. Li, J. H. Guo, T. K. Sham, X. L. Sun, *Nano Lett.* **2016**, 16, 3545.
- [73] S.-H. Jen, S. M. George, *ACS Appl. Mater. Interfaces* **2013**, 5, 1165.
- [74] S.-H. Jen, B. H. Lee, S. M. George, R. S. McLean, P. F. Garcia, *Appl. Phys. Lett.* **2012**, 101, 234103.
- [75] X. Liang, M. Yu, J. Li, Y. B. Jiang, A. W. Weimer, *Chem. Commun.* **2009**, 7140.
- [76] D. C. Miller, R. R. Foster, S.-H. Jen, J. A. Bertrand, D. Seghete, B. Yoon, Y.-C. Lee, S. M. George, M. L. Dunn, *Acta Mater.* **2009**, 57, 5083.